www.nature.com/aps

Acta Pharmacologica Sinica

ARTICLE

Gastrodin protects H9c2 cardiomyocytes against oxidative injury by ameliorating imbalanced mitochondrial dynamics and mitochondrial dysfunction

Qiao-qiao Cheng[1], Yu-wei Wan[1], Wei-min Yang[2], Meng-hua Tian[3], Yu-chuan Wang[3], Hai-yan He[3], Wei-dong Zhang[1] and Xuan Liu[1]

Gastrodin (GAS) is the main bioactive component of Tianma, a traditional Chinese medicine widely used to treat neurological disorders as well as cardio- and cerebrovascular diseases. In the present study, the protective effects of GAS on H9c2 cells against ischemia–reperfusion (IR)-like injury were found to be related to decreasing of oxidative stress. Furthermore, GAS could protect H9c2 cells against oxidative injury induced by H_2O_2. Pretreatment of GAS at 20, 50, and 100 μM for 4 h significantly ameliorated the decrease in cell viability and increase in apoptosis of H9c2 cells treated with 400 μM H_2O_2 for 3 h. Furthermore, we showed that H_2O_2 treatment induced fragmentation of mitochondria and significant reduction in networks, footprint, and tubular length of mitochondria; H_2O_2 treatment strongly inhibited mitochondrial respiration; H_2O_2 treatment induced a decrease in the expression of mitochondrial fusion factors Mfn2 and Opa1, and increase in the expression of mitochondrial fission factor Fis1. All these alterations in H_2O_2-treated H9c2 cells could be ameliorated by GAS pretreatment. Moreover, we revealed that GAS pretreatment enhanced the nuclear translocation of Nrf2 under H_2O_2 treatment. Knockdown of Nrf2 expression abolished the protective effects of GAS on H_2O_2-treated H9c2 cells. Our results suggest that GAS may protect H9c2 cardiomyocytes against oxidative injury via increasing the nuclear translocation of Nrf2, regulating mitochondrial dynamics, and maintaining the structure and functions of mitochondria.

Keywords: gastrodin; Tianma; H9c2 cardiomycytes; oxidative injury; Nrf2; mitochondrial dynamics; mitochondrial respiration

Acta Pharmacologica Sinica (2020) 41:1314–1327; https://doi.org/10.1038/s41401-020-0382-x

INTRODUCTION

Gastrodin (GAS) (*p*-hydroxymethylphenyl-b-*D*-glucopyranoside) is the main bioactive component of Rhizoma Gastrodiae (the dried rhizome of *Gastrodia elata* Blume, also known as Tianma), a popular traditional Chinese medicine. In Shennong's *Classic of Materia Medica*, the first herbal monograph in Chinese history, written during the Han Dynasty, Tianma was described as a "top grade medicine" that can rejuvenate the body, enhance health, and extend life without toxicity, and can be used long term without harm [1]. Although Tianma is traditionally used in the treatment of nervous diseases, Tianma has been reported to have protective activities against convulsion, oxidation, depression, epilepsy, obesity, asthma, and inflammation, in addition to the effects on analgesia, sedation, learning and memory improvement, and neuroprotection [2]. Tianma is currently used clinically to treat various cardiovascular and cerebrovascular diseases, as well as nervous diseases, including hypertension, headache, convulsion, epilepsy, and coronary heart diseases [3–6]. However, the mechanisms of Tianma and GAS have not been fully clarified. Furthermore, most of the previous studies on GAS focused on its effects on neurons, and little is known about the effects of GAS on cardiomyocytes.

Previous studies showed that GAS ameliorated myocardial ischemia–reperfusion (IR) injury in rats [7]. GAS pretreatment ameliorated myocardial IR injury by decreasing calcium overload [8]. GAS also protected H9c2 cardiomyocytes against injuries induced by serum deprivation [9] or LPS treatment [10]. In the present study, we examined the protective effects of GAS on H9c2 cells that underwent ischemia-like injury (deprivation of oxygen, glucose, and serum for 9 h) or IR-like injury (deprivation of oxygen, glucose, and serum for 9 h, and then culture under normal conditions in complete medium for an additional 3 h). Based on the observation of the antioxidant activity of GAS in protecting H9c2 cells against IR-like injury, we focused on studying the effects and mechanisms of GAS on H9c2 cells that underwent oxidative injury induced by H_2O_2 treatment.

Recent studies have suggested that imbalanced mitochondrial dynamics and related mitochondrial dysfunction play important roles in cardiac IR injury [11–14]. Mitochondria are highly dynamic organelles that undergo coordinated cycles of fission (to generate discrete fragmented mitochondria) and fusion (to form an interconnected elongated phenotype), referred to as "mitochondrial dynamics", to maintain their shape, distribution, and size [15, 16]. The balance of mitochondrial fusion and fission determines mitochondrial morphology, and is necessary to support mitochondrial functions. Mitochondrial dynamics are coupled to the bioenergetics and signaling functions of

[1]Institute of Interdisciplinary Integrative Biomedical Research, Shanghai University of Traditional Chinese Medicine, Shanghai 201203, China; [2]School of Pharmaceutical Science and Yunnan Key Laboratory of Pharmacology for Natural Products, Kunming Medical University, Kunming 650500, China and [3]Zhaotong Institute of Tianma, Zhaotong 657000, China
Correspondence: Wei-dong Zhang (wdzhangy@hotmail.com) or Xuan Liu (xuanliu@shutcm.edu.cn)

Received: 18 December 2019 Revised: 13 February 2020 Accepted: 14 February 2020
Published online: 12 March 2020

mitochondria. Therefore, imbalanced mitochondrial dynamics cause mitochondrial dysfunctions such as changes in mitochondrial respiration and the induction of apoptosis [17–19]. Mitochondrial dynamics may be a therapeutic target for treating cardiac diseases [14]. In the present study, we observed the morphology and functions of mitochondria in H9c2 cells under H_2O_2-induced oxidative injury with or without GAS pretreatment, and attempted to clarify the mechanisms by which GAS protects H9c2 cells against oxidative injury.

MATERIALS AND METHODS

Chemicals and materials

GAS with a purity >98% was purchased from Nature Standard Company (Shanghai, China). SRB (sulforhodamine B), TCA (trichloroacetic acid), oligomycin, FCCP (2- [2-[4-(trifluoromethoxy)phenyl]hydrazinylidene]-propanedinitrile), and rotenone were purchased from Sigma-Aldrich (St. Louis, MO, USA). MitoTracker Green FM and the Alexa Fluor 488 Annexin V/Dead Cell Apoptosis Kit were purchased from Thermo Fisher Scientific (Waltham, MA, USA). DCFH-DA (2′,7′-dichloro-fluorescin diacetate) and the bicinchoninic acid (BCA) protein assay kit were obtained from Yeasen (Shanghai, China). Antimycin A was purchased from Abcam Biotechnology (Cambridge, MA, USA). The reverse-transcription kit was obtained from TaKaRa (Shiga, Japan). The FastStart Essential DNA Green Master for PCR was purchased from Roche (Basel, Switzerland). Antibodies, except where specifically noted, were purchased from Cell Signaling Technology (Danvers, MA, USA).

Cell culture and treatments

H9c2 cells were obtained from the cell bank of the Institute of Biochemistry and Cell Biology (Shanghai, China), and cultured in Dulbecco's modified Eagle's medium (DMEM) containing 4.5 g/L *D*-glucose supplemented with 10% fetal bovine serum, 100 mg/mL streptomycin, and 100 U/mL penicillin, all bought from HyClone (Logan, Utah, USA), at 37 °C in a humidified incubator with 5% CO_2. The cells were passaged every 2 or 3 days. For treatments, H9c2 cells were seeded in 96-well plates at a density of 5×10^3 cells per well. After culturing for 24 h and reaching ~70%–80% confluence, the cells were pretreated with the indicated concentrations of GAS (dissolved in culture medium) for 4 h before induction of ischemia-like injury or IR-like injury, or treatment with H_2O_2 at the indicated concentrations. Ischemia-like or IR-like injury was induced in H9c2 cells using methods similar to those in a previous report [20]. For ischemia-like injury, the cells were deprived of oxygen, glucose, and serum for 9 h; briefly, the culture medium was replaced with serum- and glucose-free medium, and the plates were placed in an incubator with 1% O_2, 94% N_2, and 5% CO_2 air for 9 h. For IR-like injury, the cells were deprived of oxygen, glucose, and serum for 9 h, and then cultured under normal conditions in complete medium for an additional 3 h. For H_2O_2 treatment, the cells were treated with the indicated concentrations of H_2O_2 for different time periods.

Cell viability assay

Cell viability was determined using the Sulforhodamine B (SRB) assay [21]. Briefly, after treatments, the cells were fixed with cold 10% trichloroacetic acid at 4 °C for 60 min. The plates were washed five times with tap water and then air dried. SRB solution (100 μL) at 0.4% (w/v) in 1% acetic acid was added to each well and incubated at room temperature for 10 min. After staining, the plates were washed five times with 1% acetic acid to remove unbound dye and then air dried. Bound dye in the cells was subsequently solubilized with 10 mM Trizma base, and the absorbance was read using an automated plate reader at a wavelength of 515 nm. Three independent experiments (each with at least triplicate samples) were conducted, and the statistical results are shown.

Determination of the intracellular ROS level

After treatments, the cells were incubated with 10 μM DCFH-DA in serum-free and phenol red-free medium for 30 min. Then, after two phosphate-buffered saline (PBS) washes, the fluorescence intensity of each well was detected using a Cytation 5 Cell Imaging Multi-Mode Reader (BioTek, Winooski, VT, USA) at an excitation wavelength of 488 nm and an emission wavelength of 525 nm. Three independent experiments (each with triplicate samples) were conducted, and the statistical results are shown. Images of the cells were also captured with an inverted fluorescence microscope (Leica, Wetzlar, Germany).

Cell morphology observation and flow cytometric analysis of apoptosis

The morphological changes in H9c2 cells after treatments were observed with an optical microscope (DMil, Leica). For flow cytometric analysis, cells (both adherent and detached) were collected, washed with PBS, and stained by using an Alexa Fluor 488 Annexin V/Dead Cell Apoptosis Kit (Thermo Fisher Scientific) according to the manufacturer's instructions. Then, flow cytometric analysis was conducted using a FACSCalibur flow cytometer, and data analysis were performed with CellQuest software (BD Biosciences, Sparks Glencoe, MD, USA). Three independent experiments (each with triplicate samples) were conducted, and the results of one representative experiment are shown.

Mitochondrial morphology observation and network quantification

Mitochondria in living H9c2 cells were stained with 100 nM MitoTracker Green FM (Invitrogen, Carlsbad, CA, USA) for 30 min. After washing twice with PBS and transfer to phenol red-free DMEM, mitochondrial morphology was observed using a DeltaVision OMX SR imaging system with super resolution (GE Healthcare Bio-Sciences, Pittsburgh, PA, USA). The mitochondrial morphology in individual cells was quantified as described in previous reports [22, 23]. Three independent experiments were conducted, and the results of one representative experiment are shown. Briefly, random fields of cells (100 cells per condition) in each group were evaluated. The mitochondrial morphology types included long tubular, short tubular, and fragmented. The percentage of different mitochondrial morphology types in 100 cells was quantified. Furthermore, the ImageJ macro tool MiNA was used to analyze mitochondrial network morphology.

Mitochondrial respiration assay

A mitochondrial respiration assay in living cells was conducted [24] using a Seahorse XFe96 Extracellular Flux Analyzer (Seahorse Bioscience, North Billerica, MA, USA). The real-time oxygen consumption rate (OCR), which indicated the mitochondrial respiration potential of the cells, was measured. Briefly, H9c2 cells were seeded into XFe96 cell culture microplates (Seahorse Bioscience) at a density of 8000–10000 cells/well. After treatments, the culture medium was changed to unbuffered DMEM (pH 7.4) supplemented with 1 mM pyruvate, 2 mM glutamine, and 10 mM *D*-glucose at 1 h before the assay. After baseline rate measurement, oligomycin (1 μM), FCCP (1 μM), and rotenone (0.5 μM) combined with antimycin A (0.5 μM) were injected sequentially through ports in the Seahorse Flux Park cartridges. The OCR was recorded and normalized to the number of 1000 cells per well, and then the data were analyzed by using Wave Desktop Software provided by Seahorse Bioscience. Three independent experiments (each with at least triplicate samples) were conducted, and the results of one representative experiment are shown.

Transfection of siRNAs

H9c2 cells were transfected with siRNA for Nrf2 (5′-CAAACA GAATGGACCTAAA-3′) or a nontargeting siRNA, both purchased from GenePharma (Shanghai, China) by using Lipofectamine 3000 (Invitrogen) according to the manufacturer's instructions. Briefly, H9c2 cells were plated in 24- or 6-well plates and incubated until they reached 70% confluence. Lipofectamine 3000 and siRNA were mixed and incubated for 15 min at room temperature before being added to the cells. The cells were incubated with siRNA at a final concentration of 50 nM for 24 h. The expression of Nrf2 in negative control cells (cells treated with nontargeting siRNA) and Nrf2-siRNA-treated cells was evaluated using both RT-PCR and Western blot analysis.

RNA extraction and RT-PCR

Total cellular RNA was extracted using RNAiso Plus reagent (Takara, Shiga, Japan) dissolved in RNase-free water. The quantification of total RNA was conducted by detecting ultraviolet absorption (optical density, 260/280 nm) using a NanoDrop 2000 (Thermo Scientific, USA). An equal amount of total RNA (500 ng) was reverse transcribed to cDNA using PrimeScript™ RT Master Mix (Takara) according to the manufacturer's instructions. RT-PCR amplifications were performed using the FastStart Essential DNA Green Master and LightCycler® 96 Instrument (Roche, Basel, Switzerland). The thermal profile was 95 °C for 10 min, followed by 40 cycles at 95 °C for 10 s and 60 °C for 30 s. Each sample was analyzed in triplicate, and the mean cycle threshold (Ct) value was calculated. The relative expression level was calculated using the ΔΔCt method. The mRNA expression of actin was used as an internal control. Primer sequences for RT-PCR analysis are listed in Supplementary Table S1. Three independent experiments (each with at least triplicate samples) were conducted, and the statistical results are shown.

Immunofluorescence staining

After treatments, the cells were fixed in 4% paraformaldehyde for 20 min at room temperature, and then washed three times with PBS. The cells were permeabilized in 0.1% Triton X-100 (Sigma-Aldrich) for 10 min, and then blocked in 2% bovine serum albumin for 1 h at room temperature. After an overnight incubation with mouse monoclonal anti-Nrf2 antibody (#ab89443, 1:100 dilution, Abcam, Cambridge, Cambridgeshire, UK) at 4 °C, the cells were washed three times with PBS, and then incubated with secondary antibody (#A0568, FITC-labeled goat anti-mouse IgG, 1:1000 dilution, Beyotime Biotechnology) for 1 h at room temperature. Afterward, the cells were washed three times with PBS, and stained with DAPI for 10 min at room temperature. The cells were then observed using a DeltaVision OMX SR imaging system. Three independent experiments were conducted, and the results of one representative experiment are shown.

Western blotting assay

H9c2 cells were harvested and lysed in RIPA buffer containing the protease inhibitor phenylmethane-sulfonyl fluoride. The total protein concentrations were determined by using a BCA protein assay kit. Equal amounts of total proteins (20 μg) from each treatment group were separated by 10% sodium dodecyl sulfate polyacrylamide gel electrophoresis at 100 V for 2 h, and then electrophoretically transferred to polyvinylidene fluoride membranes. The membranes were blocked using TBST (1× TBS and 0.05% Tween-20) containing 5% skim milk for 2 h, and then incubated with rabbit polyclonal anti-Nrf2 (c-20) (#sc722, 1:200 dilution, Santa Cruz Biotechnology, Dallas, TX, USA) or rabbit polyclonal anti-actin (#4967S, 1:10000 dilution, Cell Signaling Technology, Danvers, MA, USA) overnight at 4 °C. After washing for 10 min in TBST (1× TBS and 0.05% Tween-20) three times, the membranes were incubated with secondary polyclonal antibody (goat anti-rabbit HRP-conjugated IgG, 1:10000 dilution, Absin, Shanghai, China) for 1 h at room temperature. After the membranes were washed again in TBST, the immune complexes were detected by using ECL-Plus™ chemiluminescent detection reagent (P0018A, Beyotime Biotechnology), and visualized with a Molecular ImagerR ChemiDoc™ XRS + System (Bio-Rad Laboratories, Hercules, CA, USA). Three independent experiments were conducted, and the results of one representative experiment are shown.

Statistical analysis

Values are expressed as the mean ± standard deviation. All statistical analyses were performed using GraphPad Prism 5.0 software, and comparisons between two groups were analyzed using two-tailed Student's *t* test. A *P* value less than 0.05 was considered statistically significant.

RESULTS

GAS protected H9c2 cells against ischemia-like injury, IR-like injury, and H_2O_2-induced injury

As shown in Fig. 1a, treatment with GAS at concentrations ranging from 5 to 100 μM exhibited no significant influence on the viability of H9c2 cells. As shown in Supplementary Fig S1, pretreatment with GAS significantly protected H9c2 cells against ischemia-like injury (Fig S1a), as well as IR-like injury (Fig S1b). Intracellular reactive oxygen species (ROS)-level measurements indicated that the increase in intracellular ROS induced by IR-like injury was significantly ameliorated by GAS pretreatment (Fig S1c). These results suggest that GAS-mediated protection of H9c2 cells against IR-like injury is related to a decrease in oxidative stress. Therefore, the present study focused on studying the effects of GAS on H9c2 cells that underwent oxidative injury induced by H_2O_2 treatment.

First, the viability of H9c2 cells treated with different concentrations of H_2O_2 for 24 h (Fig. 1b) was observed. As shown in Fig. 1b, H_2O_2 at 200, 300, 400, and 500 μM induced ~10%, 30%, 60%, and 80% decreases in the viability of H9c2 cells, respectively. To determine the conditions in which cell viability would decrease by ~40% or 50% in less than 24 h, the effect of 400 μM GAS treatment for different times (3, 6, 9, and 24 h) on cell viability was further examined. As shown in Fig. 1c, treatment with 400 μM H_2O_2 for 3 h induced an approximately 40% decrease in cell viability, and thus was used as a condition for H_2O_2 treatment in the subsequent experiments. As shown in Fig. 1d, pretreatment with GAS at 20, 50, and 100 μM significantly ameliorated the decrease in viability in H_2O_2-treated H9c2 cells. Intracellular ROS-level measurements indicated that the H_2O_2-induced increase in ROS was significantly ameliorated by GAS pretreatment (Fig. 1e). Representative photographs of the intracellular ROS signal in H9c2 cells treated with 400 μM H_2O_2 for 3 h with or without GAS pretreatment (Fig. 1f) also show that GAS pretreatment inhibited the H_2O_2-induced increase in intracellular ROS. These results suggest that GAS protects H9c2 cells against H_2O_2-induced oxidative injury.

GAS attenuated H_2O_2-induced apoptosis of H9c2 cells

Representative photographs of cultured H9c2 cells treated with 400 μM H_2O_2 with or without GAS pretreatment are shown in Fig. 2a. Treatment with H_2O_2 induced considerable cell death in H9c2 cells, while GAS pretreatment ameliorated H_2O_2-induced cell death (Fig. 2a). Flow cytometry results showed that H_2O_2-induced cell death included both early and late apoptosis (Fig. 2b). The cells that were Annexin V-FITC$^+$/PI$^-$ were defined as early apoptotic cells, while the cells that were Annexin V-FITC$^+$/PI$^+$ were defined as late apoptotic cells. As shown in the quantification of the flow cytometry results, GAS significantly decreased the percentage of apoptotic cells (Fig. 2c). These results suggest that GAS attenuates H_2O_2-induced apoptosis in H9c2 cells. Notably, no

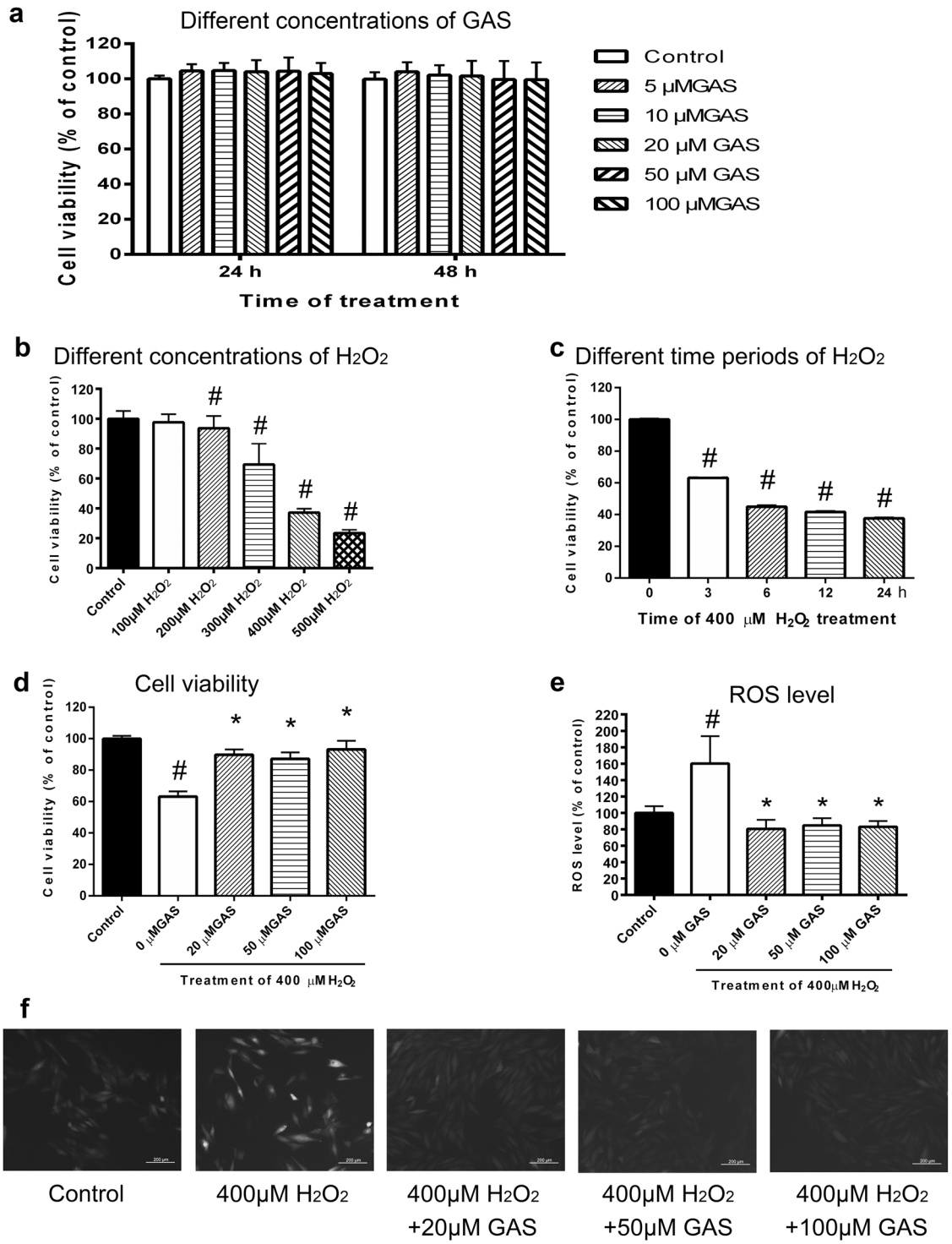

Fig. 1 GAS protected H9c2 cells against H_2O_2-induced injury. **a** Viability of H9c2 cells treated with different concentrations of GAS for 24 or 48 h. **b** Viability of H9c2 cells treated with different concentrations of H_2O_2 for 24 h. **c** Viability of H9c2 cells treated with 400 μM H_2O_2 for different times. **d** Viability of H9c2 cells treated with 400 μM H_2O_2 for 3 h with or without GAS pretreatment. **e** Intracellular ROS levels of H9c2 cells treated with 400 μM H_2O_2 for 3 h with or without GAS pretreatment. **f** Representative images of intracellular ROS levels in the different groups of cells. Bar = 200 μm. The data presented are the mean ± SD of triplicate-independent experiments. $^{\#}P < 0.05$ vs. the control group, $^{*}P < 0.05$ vs. the H_2O_2-induced group

obvious dose–response effect of GAS was observed in either the apoptosis or cell viability analysis (as shown in Fig. 1d). The reason for this is unclear. It is possible that the protective effects of GAS on H9c2 cells were mainly due to decreasing ROS levels, and the response to ROS elimination might plateau.

GAS attenuated imbalanced mitochondrial dynamics in H9c2 cells induced by H_2O_2

Representative photographs of mitochondrial morphology in control cells, cells treated with 400 μM H_2O_2, and cells treated with both 400 μM H_2O_2 and 50 μM GAS pretreatment are shown in

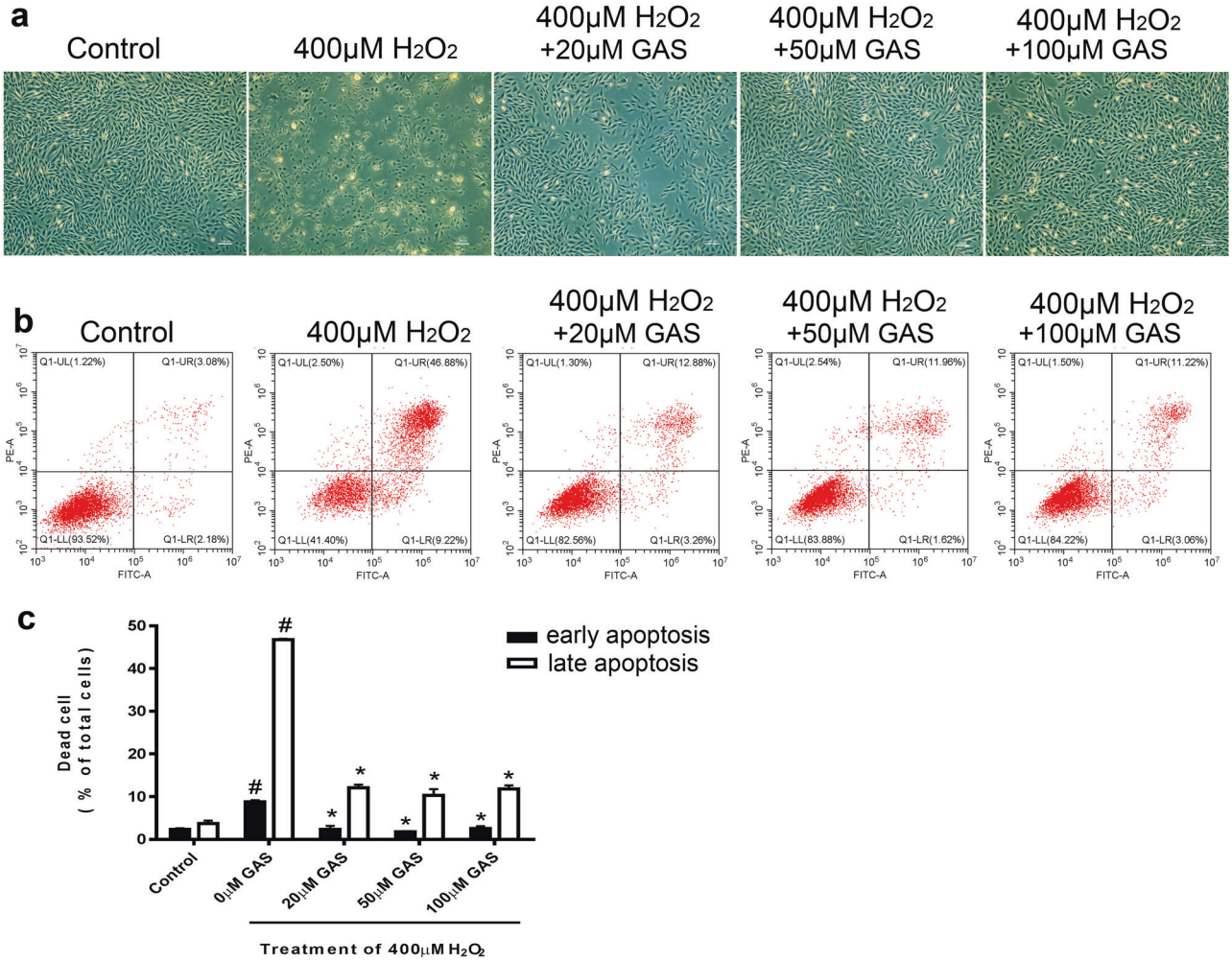

Fig. 2 GAS attenuated apoptosis of H9c2 cells induced by H_2O_2. **a** Representative photographs of H9c2 cells treated with 400 μM H_2O_2 for 3 h with or without GAS pretreatment. Bar = 200 μm. **b** Representative flow cytometry results showing apoptosis of H9c2 cells by using an Annexin V-FITC/PI double-staining assay. **c** Quantitative results of the percentage of early and late apoptotic H9c2 cells. The data presented are the mean ± SD and $^{\#}P < 0.05$ vs. the control group, $^{*}P < 0.05$ vs. the H_2O_2-induced group

Fig. 3a. As shown in Fig. 3a, mitochondria in control H9c2 cells exhibited normal, long tubular structures, while mitochondria in H_2O_2-treated H9c2 cells exhibited mostly short tubular or fragmented structures. GAS pretreatment partly ameliorated the H_2O_2-induced fragmentation of mitochondria (Fig. 3a). Quantification of 100 random cells in each group confirmed that GAS significantly ameliorated the decrease in the percentage of cells with long tubular mitochondria, and the increase in the percentage of cells with short tubular mitochondria or fragmented mitochondria induced by H_2O_2 (Fig. 3b). Mitochondrial network morphology characteristic analyses using the ImageJ macro tool MiNA are shown in Fig. 3c–g. GAS significantly attenuated the H_2O_2-induced change in networks (Fig. 3c), mitochondrial footprint (Fig. 3e), and mean branch length (Fig. 3f). These results suggest that H_2O_2 treatment induces considerable imbalance in mitochondrial dynamics in H9c2 cells, while GAS pretreatment partly attenuates the H_2O_2-induced change in mitochondrial morphology, and might be helpful in maintaining mitochondrial function.

GAS attenuated mitochondrial dysfunction in H9c2 cells induced by H_2O_2

The mitochondrial respiration potency of H9c2 cells treated with H_2O_2 with or without GAS pretreatment was measured. As shown in Fig. 4a, H_2O_2 treatment induced a considerable decrease in mitochondrial respiration potency. Treatment with GAS alone exhibited no influence on mitochondrial respiration, while pretreatment with GAS partly ameliorated the H_2O_2-induced inhibition of mitochondrial respiration in H9c2 cells (Fig. 4a). Analysis of the mitochondrial respiration parameters, such as basal respiration, maximal respiration, and ATP production, are shown in Fig. 4b–d, respectively. GAS pretreatment significantly ameliorated the H_2O_2-induced decrease in basal respiration (Fig. 4b), maximal respiration (Fig. 4c), and ATP production (Fig. 4d) in H9c2 cells. These results suggest that H_2O_2-induced mitochondrial dysfunction in H9c2 cells was partly attenuated by GAS.

GAS induced nuclear translocation of the Nrf2 protein in H9c2 cells

As shown in Fig. 5a, the Western blotting results showed that H_2O_2 treatment with or without GAS pretreatment did not cause a significant change in the protein level of Nrf2. The Nrf2 protein only showed a slight increase in cells that were treated with GAS. Interestingly, as shown in Fig. 5b, the distribution of Nrf2 protein in H9c2 cells exhibited great differences in the different groups of cells. In control cells, Nrf2 protein was almost exclusively observed in the cytoplasm. Treatment with H_2O_2 induced translocation of Nrf2 protein from the cytoplasm into the nucleus, which indicated activation of Nrf2; therefore, the yellow signal (merge of the red signal of Nrf2 and the green signal of nuclear DAPI staining)

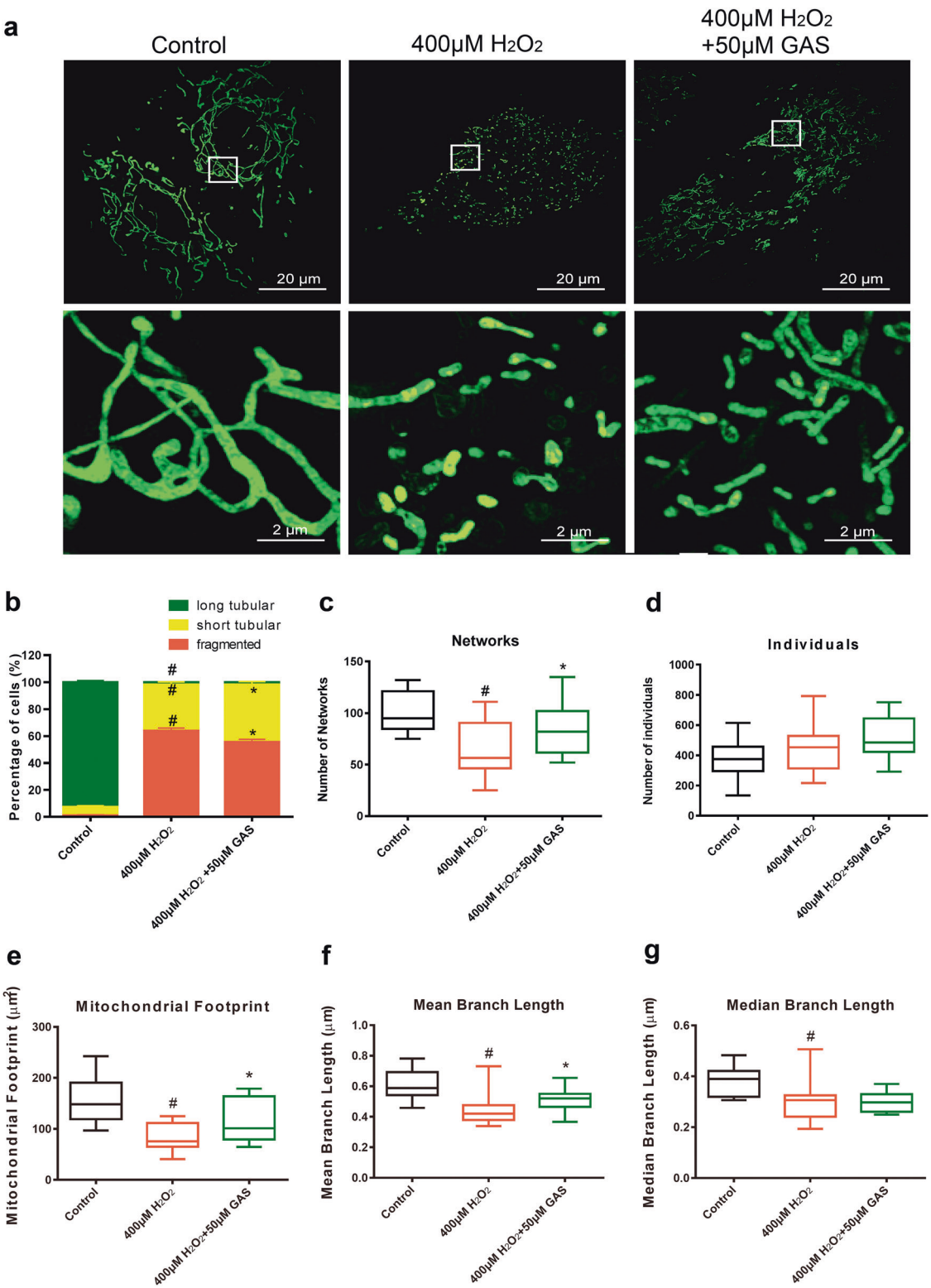

Fig. 3 GAS attenuated the imbalanced mitochondrial dynamics of H9c2 cells induced by H_2O_2. **a** Representative photographs of mitochondrial morphology in H9c2 cells treated with 400 μM H_2O_2 for 3 h with or without GAS pretreatment. Bar = 20 or 2 μm. **b** Quantitative results of the percentage of cells with long tubular mitochondria, short tubular mitochondria, or fragmented mitochondria. **c**–**g** Quantitative results of mitochondrial network characteristics, including networks (**c**), individuals (**d**), mitochondrial footprint (**e**), mean branch length (**f**), and median branch length (**g**). The data presented are the mean ± SD and $^{\#}P < 0.05$ vs. the control group, $^{*}P < 0.05$ vs. the H_2O_2-induced group

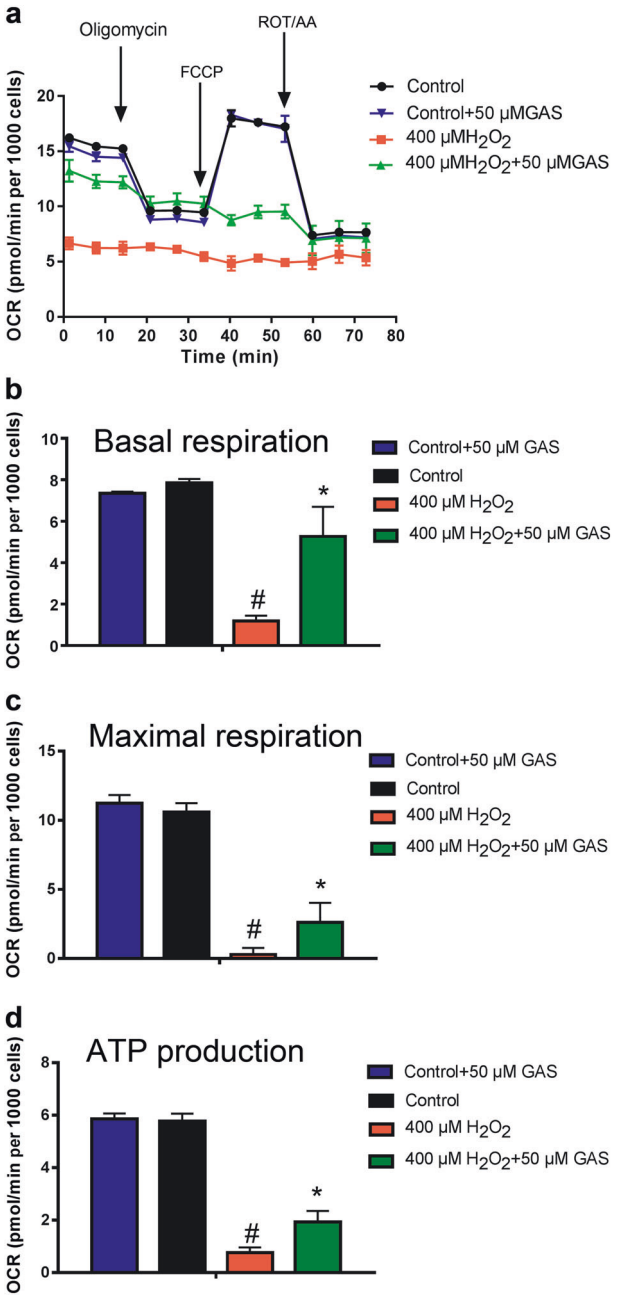

Fig. 4 GAS attenuated mitochondrial dysfunction in H9c2 cells induced by H_2O_2. **a** Mitochondrial respiration potency of control cells, 50 μM GAS-treated cells, and 400 μM H_2O_2-treated cells, pretreated with 50 μM GAS, was measured using a Seahorse metabolic analyzer. **b** Results of quantification analysis of basal respiration. **c** Results of quantification analysis of maximal respiration. **d** Results of quantification analysis of ATP production. The data presented are the mean ± SD and $^{\#}P < 0.05$ vs. the control group, $^{*}P < 0.05$ vs. the H_2O_2-induced group

increased in these cells. Importantly, pretreatment with GAS enhanced the nuclear translocation of Nrf2, and the cells exhibited a strong yellow signal, which suggested that GAS induced activation of Nrf2 in H9c2 cells (Fig. 5b).

Nrf2 was involved in the protective effects of GAS on H_2O_2-treated H9c2 cells

To examine whether Nrf2 was involved in the protective effects of GAS on H9c2 cells, Nrf2 expression in H9c2 cells was knocked down using siRNA transfection, and then the effects of GAS on these Nrf2-siRNA-treated cells were compared with the effects on negative control cells (cells treated with nontargeting siRNA). As shown in Fig. 6a (RT-PCR results) and Fig. 6b (Western blotting results), Nrf2-siRNA transfection successfully decreased both the mRNA and protein expression of Nrf2 in H9c2 cells. In negative control cells, H_2O_2 treatment induced a significant decrease in cell viability, while GAS pretreatment significantly ameliorated the H_2O_2-induced decrease (Fig. 6c). In contrast, in Nrf2-siRNA-treated cells, H_2O_2 treatment also induced a significant decrease in cell viability, but GAS pretreatment did not ameliorate the H_2O_2-induced decrease in cell viability (Fig. 6c). Analysis of intracellular ROS levels showed similar results: in Nrf2-siRNA-treated cells, GAS pretreatment did not ameliorate the H_2O_2-induced increase in ROS levels (Fig. 6d). These results suggest that Nrf2 knockdown attenuated the protective effects of GAS against oxidative stress, and that Nrf2 is involved in the mechanisms of GAS.

Knockdown of Nrf2 expression attenuated the effects of GAS on H_2O_2-induced imbalanced mitochondrial dynamics

As shown in Fig. 7a, in negative control cells, H_2O_2 treatment induced imbalanced mitochondrial dynamics, while GAS pretreatment ameliorated the imbalanced mitochondrial dynamics induced by H_2O_2. In contrast, in Nrf2-siRNA-treated cells, GAS pretreatment did not successfully ameliorate the imbalanced mitochondrial dynamics induced by H_2O_2 (Fig. 7b). Quantitative analysis of mitochondrial network characteristics showed similar results: in Nrf2-siRNA-treated cells, GAS pretreatment did not ameliorate the decrease in mitochondrial footprint, mean branch length, or median branch length induced by H_2O_2 (Fig. 7c). These results suggest that Nrf2 is involved in the effects of GAS in maintaining the mitochondrial morphology of H9c2 cells that underwent H_2O_2 treatment.

GAS inhibited H_2O_2-induced changes in expression levels of genes related to mitochondrial fusion and fission

As shown in Fig. 8a, in negative control cells, H_2O_2 treatment induced significant changes in the expression levels of genes related to mitochondrial fusion (Mfn1, Mfn2, and Opa1) and mitochondrial fission (Fis1 and Drp1). GAS pretreatment significantly ameliorated the changes in the expression levels of Mfn2, Opa1, and Fis1, but did not influence those of Mfn1 and Drp1 (Fig. 8a). These results suggest that Mfn2, Opa1, and Fis1 play roles in the protective effects of GAS on the mitochondria of H9c2 cells. Furthermore, as shown in Fig. 8b, Nrf2 knockdown attenuated the regulatory effects of GAS on the expression levels of Mfn2, Opa1, and Fis1. These results confirmed the involvement of Nrf2 in the mechanisms of GAS. To determine whether Nrf2 knockdown directly affects the expression levels of these genes related to mitochondrial fusion and fission, the expression levels of the genes in negative control cells and Nrf2-siRNA-treated cells were also compared. As shown in Fig. 8c, Nrf2 knockdown significantly decreased the expression level of Mfn2 but not that of Opa1 or Fis1. These results suggest that Nrf2 has direct regulatory effects on mitochondrial fusion.

Knockdown of Nrf2 expression attenuated the effects of GAS on H_2O_2-induced mitochondrial dysfunction

As shown in Fig. 9a, in negative control cells, H_2O_2 treatment induced a considerable decrease in mitochondrial respiration potency, while GAS pretreatment partly ameliorates the H_2O_2-induced mitochondrial dysfunction. Treatment with Nrf2-siRNA induced a slight decrease in mitochondrial respiration potency. Importantly, in Nrf2-siRNA-treated cells, H_2O_2 treatment also induced a considerable decrease in mitochondrial respiration potency, but GAS pretreatment did not ameliorate the H_2O_2-induced mitochondrial dysfunction (Fig. 9a). Analysis of the parameters of mitochondrial respiration, such as basal respiration, maximal respiration, and ATP production, are shown in Fig. 9b–d,

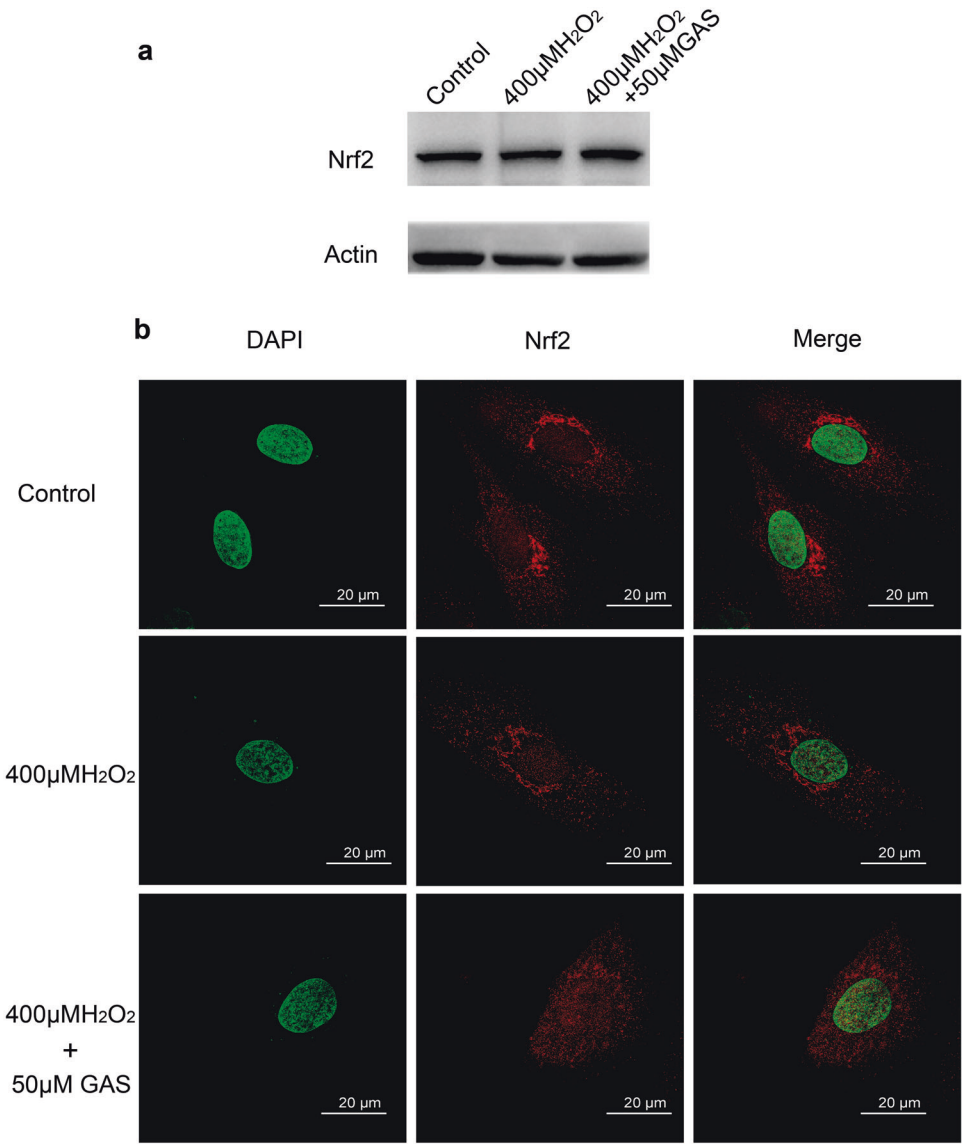

Fig. 5 GAS induced nuclear translocation of Nrf2 in H9c2 cells. **a** Western blotting results showing Nrf2 protein in control and H_2O_2-treated cells with GAS pretreatment. Actin was used as the loading control. **b** Representative results of immunofluorescence staining of the intracellular distribution of Nrf2 protein in H9c2 cells. Bar = 20 μm

respectively. In Nrf2-siRNA-treated cells, GAS pretreatment did not ameliorate the decrease in basal respiration (Fig. 9b), maximal respiration (Fig. 9c), or ATP production (Fig. 9d) induced by H_2O_2. These results suggest that Nrf2 is involved in the effects of GAS in maintaining the mitochondrial functions of H9c2 cells that underwent H_2O_2 treatment.

DISCUSSION

In the present study, GAS protected H9c2 cells against ischemia-like and IR-like injury. The results were consistent with previous reports about the cardioprotective effects of GAS [7–9, 25]. Importantly, the protective effects of GAS against IR-like injury were found to be related to its ROS-decreasing activity, and GAS directly protected H9c2 cells against oxidative injury (H_2O_2 treatment). The antioxidant effects of GAS have also been observed in other types of cells, such as neurons [26, 27], astrocytes [28], osteoblasts [29], bone marrow mesenchymal stem cells, and macrophages [30]. These results suggest that antioxidant activity plays important roles in the various effects of GAS.

Mitochondria are especially important in cardiomyocytes, since the heart is an organ with high bioenergetic demands, and more than 90% of ATP is supplied by mitochondria [31]. Interestingly, mitochondria are highly dynamic organelles with constant movement and morphological changes. Mitochondrial dynamics are involved in fundamental biological processes such as cell metabolism, cell survival, and death [31]. Our results in observing the morphology of mitochondria by using super resolution microscopy showed that H_2O_2 treatment induced fragmentation of mitochondria, and a significant decrease in networks, footprints, and tubular lengths of mitochondria in H9c2 cells. Disruption of mitochondrial dynamics has been implicated in various human diseases, including developmental defects, neurodegenerative diseases, metabolic diseases, and cardiovascular diseases [31]. Previous reports have shown that mitochondrial morphological defects, such as increased mitochondrial fission and decreased fusion, are important events in cardiac ischemia and reperfusion [32–35]. For example, fragmented mitochondria and a decrease in mitochondrial fusion were detected in cardiomyocytes from both heart failure patients

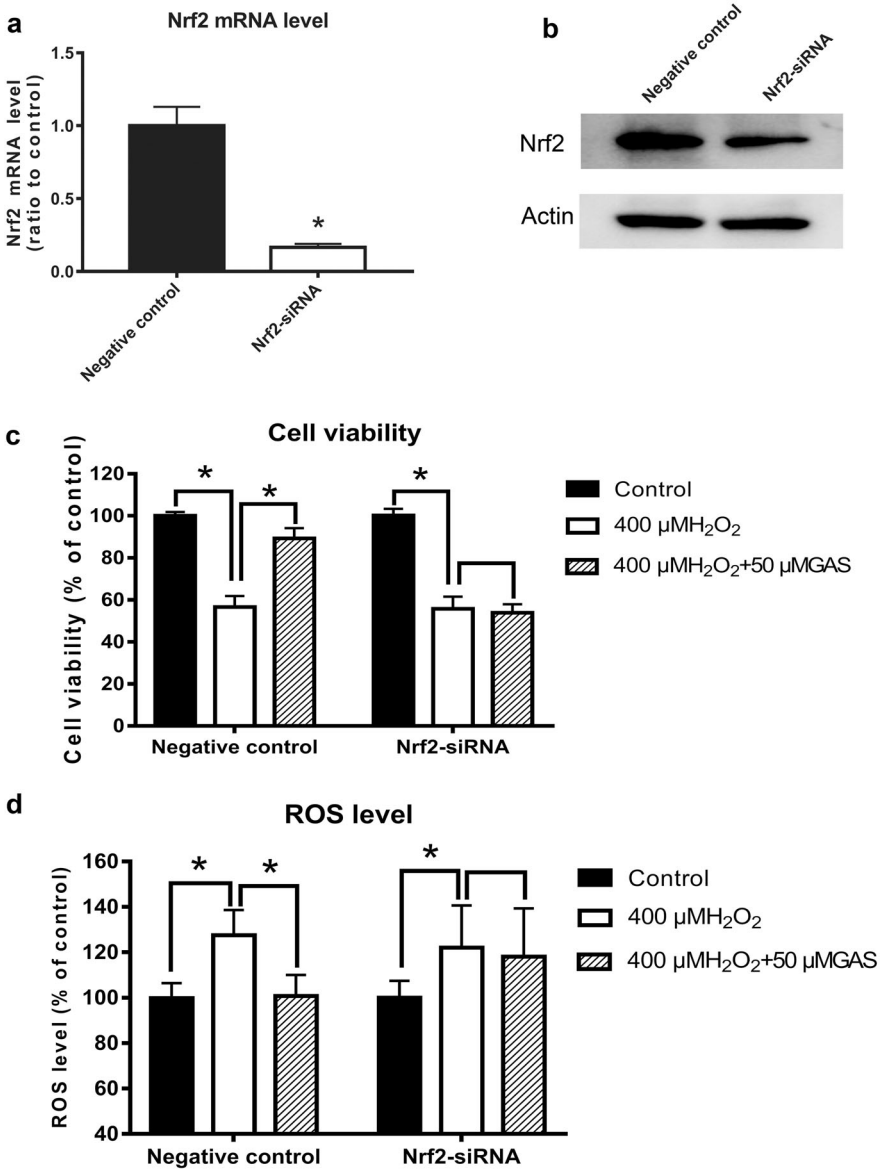

Fig. 6 Knockdown of Nrf2 expression attenuated the protective effects of GAS on H_2O_2-treated H9c2 cells. **a** RT-PCR results showing Nrf2 mRNA expression levels in negative control cells (cells treated with nontargeting siRNA) and cells treated with Nrf2-siRNA. **b** Western blotting results showing Nrf2 protein expression levels in negative control cells and Nrf2-siRNA-treated cells. **c** Viability of negative control cells or Nrf2-siRNA-treated cells subjected to 400 μM H_2O_2 treatment with or without GAS pretreatment. **d** Intracellular ROS levels of negative control cells or Nrf2-siRNA-treated cells subjected to 400 μM H_2O_2 treatment with or without GAS pretreatment. The data presented are the mean ± SD of three independent experiments. *$P < 0.05$ between the indicated two groups

and cardiac ischemia animal models [35]. The results of the present study clearly showed imbalanced mitochondrial dynamics in H_2O_2-treated H9c2 cells, as indicated by a decrease in mitochondrial fusion and an increase in mitochondrial fission. Furthermore, GAS ameliorated the imbalanced mitochondrial dynamics induced by H_2O_2. The effects of GAS in maintaining the normal structure of mitochondria might be the basis for protecting H9c2 cells against oxidative injury. Cell apoptosis is closely related to mitochondrial dynamics. During apoptosis, mitochondria undergo extensive fragmentation, which precedes caspase activation, to release proapoptotic factors [36]. Excessive fission or decreased fusion contributes to cell apoptosis, while inhibition of mitochondrial fission blocks or delays cell death [37–40]. The GAS-mediated protection of mitochondria from fragmentation might contribute to the decrease in apoptosis in H_2O_2-treated H9c2 cells that were pretreated with GAS.

Mitochondrial dynamics and bioenergetics are reciprocally coupled [17]; thus, imbalanced mitochondrial dynamics might result in dysfunctional mitochondrial respiration and ATP production. Measurement of real-time mitochondrial respiration in living H9c2 cells using a Seahorse XFe96 Extracellular Flux Analyzer showed that mitochondrial respiration in H9c2 cells, including basal respiration, maximal respiration, and ATP production, was strongly inhibited by H_2O_2 treatment. GAS treatment alone did not affect mitochondrial respiration, while pretreatment with GAS partly ameliorated the H_2O_2-induced inhibition of mitochondrial respiration. Previous reports have shown that elongated mitochondria are linked to more efficient ATP production and distribution, and better sustained stress-induced cell damage, while fragmented (through fission) mitochondria are associated with decreased ATP production and increased susceptibility to injury [41, 42]. The protective effects of GAS on mitochondrial

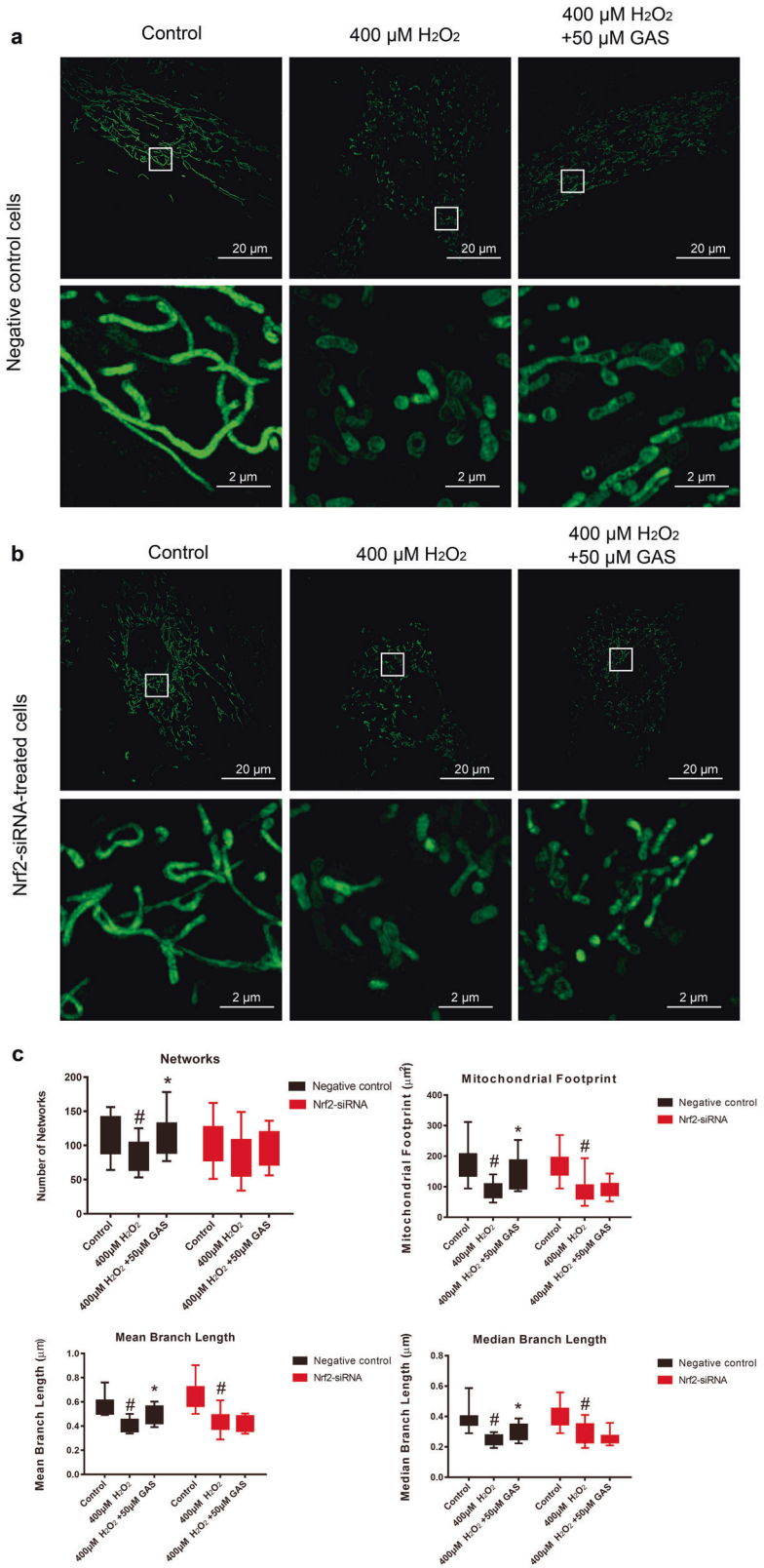

Fig. 7 Knockdown of Nrf2 expression attenuated the effects of GAS on H_2O_2-induced imbalanced mitochondrial dynamics in H9c2 cells. **a** Representative photographs of mitochondrial morphology in negative control H9c2 cells treated with 400 μM H_2O_2 for 3 h with or without GAS pretreatment. Bar = 20 or 2 μm. **b** Representative photographs of mitochondrial morphology in Nrf2-siRNA-treated H9c2 cells treated with 400 μM H_2O_2 for 3 h with or without GAS pretreatment. Bar = 20 or 2 μm. **c** Quantitative results of the mitochondrial network characteristics, including networks, mitochondrial footprint, mean branch length, and median branch length. The data presented are the mean ± SD and $^{\#}P < 0.05$ vs. the control group, $^{*}P < 0.05$ vs. the H_2O_2-induced group

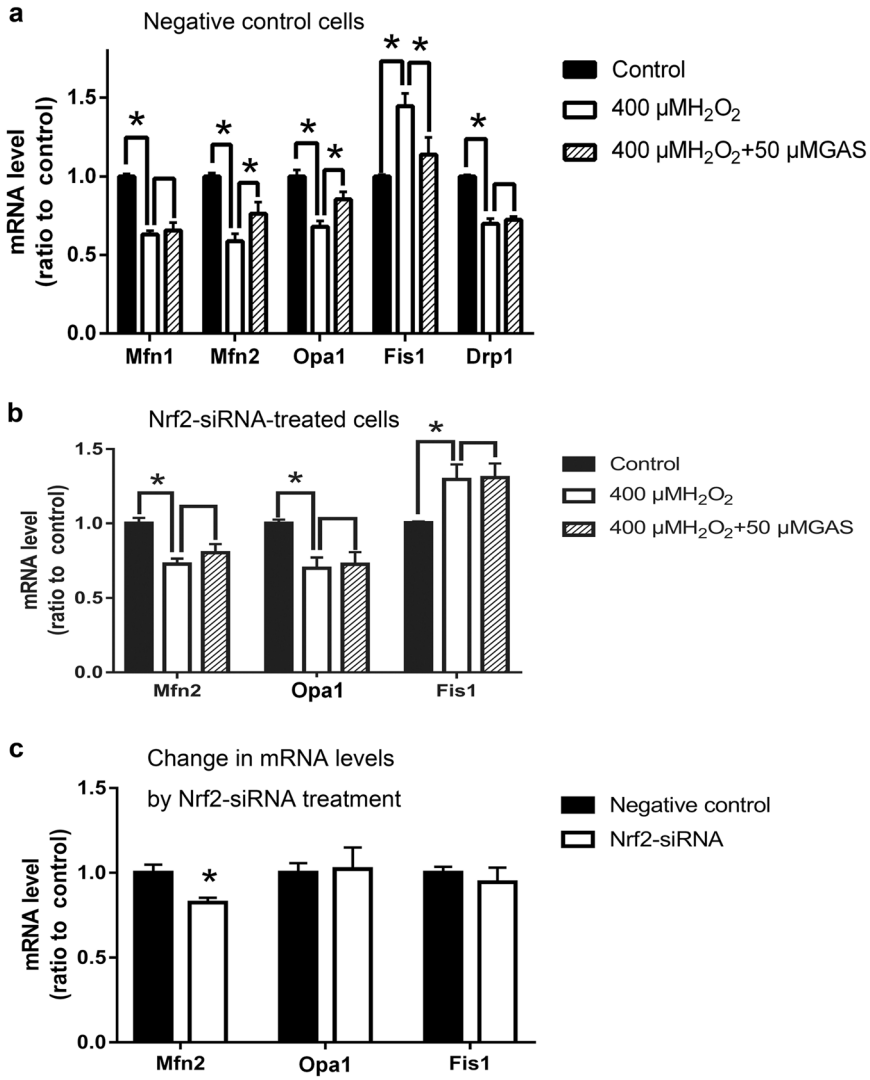

Fig. 8 Expression levels of genes related to mitochondrial fusion and fission in negative control cells and Nrf2-siRNA-treated cells that underwent H_2O_2 treatment. **a** RT-PCR results showing the expression levels of Mfn1, Mfn2, Opa1, Fis1, and Drp1 in negative control cells that underwent H_2O_2 treatment with or without GAS pretreatment. **b** RT-PCR results showing the expression levels of Mfn2, Opa1, and Fis1 in Nrf2-siRNA-treated cells that underwent H_2O_2 treatment with or without GAS pretreatment. **c** Comparison of the expression levels of Mfn2, Opa1, and Fis1 in negative control cells and Nrf2-siRNA-treated cells. The data presented are the mean ± SD of at least three independent experiments. *$P < 0.05$ between the indicated two groups

respiration and ATP production might be related to its regulatory effects on mitochondrial dynamics and mitochondrial fragmentation. Notably, accumulating evidence supports that mitochondrial dynamics and bioenergetics may reciprocally influence each other, depending on the experimental condition or initial stimulation [17]. The interaction and feedback regulation between mitochondrial dynamics and mitochondrial respiration might be involved in the mechanisms of GAS.

Mitochondrial dynamics are controlled by a group of proteins, such as the fusion proteins mitofusin 1 and 2 (Mfn1/2) and optic atrophy 1 (Opa1), and the fission proteins fission protein 1 (Fis1) and dynamin-related protein 1 (Drp1). Mitochondrial fusion is an essential mechanism by which damaged mitochondria mitigate stresses by exchanging proteins, lipids, and mitochondrial DNA with healthy mitochondria [17]. Mfn1 and Mfn2 are the primary regulators of outer mitochondrial membrane fusion, while Opa1 mediates inner mitochondrial membrane fusion [43, 44]. The present study showed that H_2O_2 treatment induced a significant decrease in the expression of Mfn1, Mfn2, and Opa1. These results suggest that both outer and inner mitochondrial membrane fusion were inhibited by H_2O_2 treatment. GAS pretreatment significantly ameliorated the decrease in the expression levels of Mfn2 and Opa1, but not Mfn1 in H_2O_2-treated H9c2 cells. Mitochondrial fission is also critical in mitochondrial quality control by separating damaged mitochondria and subsequently removing them through mitophagy [17]. In yeast, mitochondrial fission is regulated by cytosolic dynamin-like GTPase (Dnm1p) and a C-tail-anchored outer membrane protein, Fis1p. In mammals, Drp1 and Fis1 are involved in mitochondrial fission as Dnm1 and Fis1 orthologs, respectively [45]. Fis1, located on the mitochondrial outer membrane, recruits Drp1 from the cytosol to the outer mitochondrial membrane, and then the GTPase activity of Drp1 provides a driving force through hydrolyzing GTP to mediate outer and inner mitochondrial membrane fission [46, 47]. The present study showed that H_2O_2 treatment induced a significant increase in the expression of Fis1 and a decrease in Drp1. The increase in Fis1, a mitochondrial fission-stimulating protein [45], indicates activation of the mitochondrial fission process in H_2O_2-treated H9c2 cells. The decrease in Drp1 is interesting, although the mechanism for its decrease is unknown. A previous report

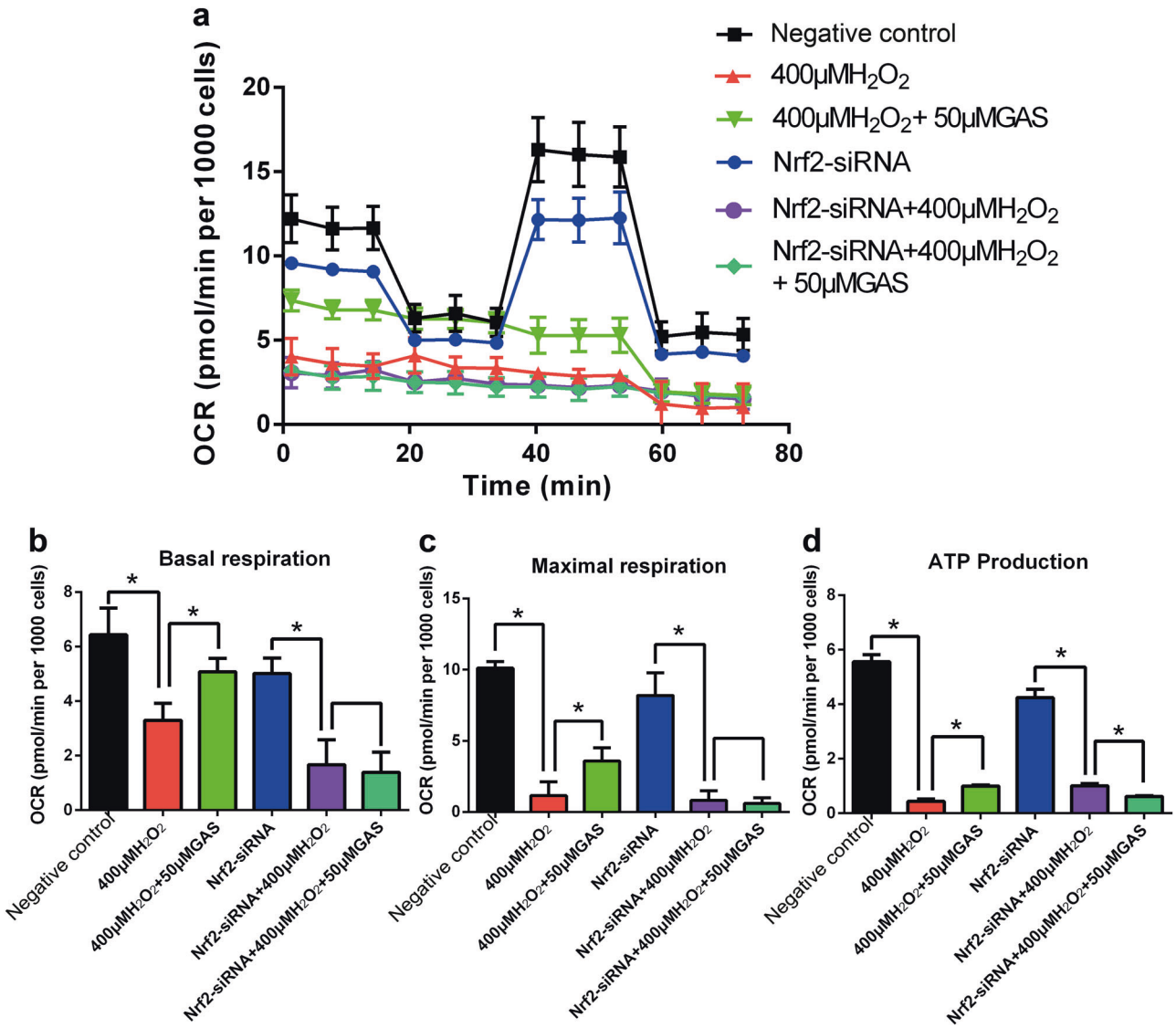

Fig. 9 Knockdown of Nrf2 expression attenuated the effects of GAS on H_2O_2-induced mitochondrial dysfunction in H9c2 cells. **a** Mitochondrial respiration potency in negative control cells or Nrf2-siRNA-treated cells that underwent H_2O_2 treatment with or without pretreatment with 50 μM GAS. **b** Results of quantification analysis of basal respiration. **c** Results of quantification analysis of maximal respiration. **d** Results of quantification analysis of ATP production. The data presented are the mean ± SD and $^*P < 0.05$ between the indicated two groups

examining the expression of Drp1 in H9c2 cells and 143B osteosarcoma cells also showed that under H_2O_2 treatment, Drp1 expression significantly decreases in H9c2 cells and slightly decreased in 143B cells [48]. The roles of Drp1 in oxidative stress-induced cells need further study. GAS pretreatment ameliorated the increase in Fis1, but exhibited no influence on the expression of Drp1. These results suggest that GAS ameliorated the activation of mitochondrial fission induced by H_2O_2.

The present study confirmed that nuclear factor erythroid 2-related factor 2 (Nrf2) is an important target of GAS. Nrf2 is a transcription factor that is activated by increased ROS production, and reduces ROS levels by upregulating antioxidant/detoxification genes [49]. Activation of Nrf2, including an increase in expression and/or nuclear translocation, has been observed in various types of cells treated with H_2O_2 in time- and dose-dependent manners [50, 51]. In the present study, treatment with H_2O_2 at 400 μM for 3 h induced the nuclear translocation of Nrf2 without a significant increase in the Nrf2 expression level. Importantly, GAS pretreatment resulted in a slight increase in Nrf2 expression, and strongly enhanced the nuclear translocation of Nrf2 under H_2O_2 treatment. The roles of Nrf2 in the mechanisms of GAS have been reported in neurons [27, 28, 52–57], osteoblasts [29, 58], liver HL-7702 cells [59], and endothelial cells [60]. In the present study, knockdown of Nrf2 expression attenuated the protective effects of GAS on H9c2 cells, as indicated by increasing cell viability, decreasing ROS levels, ameliorating mitochondrial fragmentation, and maintaining mitochondrial respiration potency. These results suggest that Nrf2 is also an important target of GAS in H9c2 cardiomyocytes, and plays critical roles in the protective effects of GAS against oxidative injury. Furthermore, Nrf2 knockdown also attenuated the effects of GAS on the expression of mitochondrial fusion- and fission-related genes such as Mfn2, Opa1, and Fis1. Nrf2 knockdown also directly influenced the expression of Mfn2 in H9c2 cells. These results suggest that Nrf2 contributes to the control of mitochondrial dynamics.

In summary, GAS induces the activation of Nrf2, regulates mitochondrial dynamics, maintains the structure and functions of mitochondria, and thus protects H9c2 cells against oxidative

injury. There has been a renaissance in mitochondrial research in recent years, featuring exciting developments in understanding the structure and organization of mitochondria, and the roles of mitochondria in cellular-signaling mechanisms, in addition to their traditional role as a cell powerhouse in eukaryotes [17]. The canonical and noncanonical roles of mitochondrial dynamics factors, such as Mfn1/2, Opa1, Fis1, and Drp1, suggested by recent discoveries, have added another dimension to the integration of mitochondrial functions [17]. In addition to the canonical roles of these factors in controlling the fusion/fission of mitochondria, they might also bear noncanonical roles, such as regulating mitochondrial bioenergetics and cell death, including apoptosis and autophagy [35, 37, 61]. Through dynamic changes in structure, mitochondria play important and pleiotropic roles in cells by regulating ATP production, ROS levels, ion channels, cell survival, and death under physiological conditions, as well as under injury. The present study suggests that the regulation of mitochondria is involved in GAS-mediated protection of H9c2 cardiomyocytes, and confirmed the critical role of mitochondria in cell regulation under oxidative injury. However, the mechanisms of mitochondrial dynamics regulation have not been fully clarified, and further study in this area is necessary and important.

ACKNOWLEDGEMENTS

This work was supported by the Chen-Kai-Xian Academician Workstation in Yunnan Province (No. 2017IC041), National Natural Science Foundation of China (Nos. 81873056 and 81872496), and the Open Project of the State Key Laboratory of Innovative Natural Medicine and Traditional Chinese Medicine Injections (No. QFSKL2018006).

AUTHOR CONTRIBUTIONS

QQC conducted the experiments, analyzed the data, and drafted the paper. YWW participated in the experiments. WMY, MHT, YCW, and HYH helped to design the experiments. WDZ and XL supervised the research and revised the paper. All authors reviewed and approved the paper.

ADDITIONAL INFORMATION

The online version of this article (https://doi.org/10.1038/s41401-020-0382-x) contains supplementary material, which is available to authorized users.

Competing interests: The authors declare no competing interests.

REFERENCES

1. Liu Y, Gao J, Peng M, Meng H, Ma H, Cai P, et al. A review on central nervous system effects of gastrodin. Front Pharmacol. 2018;9:24.
2. Wu J, Wu B, Tang C, Zhao J. Analytical techniques and pharmacokinetics of gastrodia elata blume and its constituents. Molecules. 2017;22:E1137.
3. Feng L, Manavalan A, Mishra M, Sze SK, Hu JM, Heese K. Tianma modulates blood vessel tonicity. Open Biochem J. 2012;6:56–65.
4. Cheng Q, Yang W, Liu M. Research progress on pharmacological mechanism of Gastrodiae Rhizoma in Cardiovascular and metabolic diseases. Acad J Shanghai Univ Trad Chin Med. 2019;33:96–100.
5. Jiang J, Huang D, Li Y, Gan Z, Li H, Li X, et al. Heart protection by herb formula BanXia BaiZhu TianMa decoction in spontaneously hypertensive rats. Evid Based Complement Altern Med. 2019;2019:5612929.
6. Chen B, Wang Y, He Z, Wang D, Yan X, Xie P. Tianma Gouteng decoction for essential hypertension: protocol for a systematic review and meta-analysis. Evid Based Complement Altern Med. 2018;97:e9972.
7. Wei Y, Lin T, Jiawang D, Song L, Jian Y, Hui W, et al. Protective effect of gastrodin pretreatment on myocardial ischemia reperfusion injury. J Clin Cardiol. 2017;33:381–5.
8. Li Y, Wang X, Lou C. Gastrodin pretreatment impact on sarcoplasmic reticulum calcium transport ATPase (SERCA) and calcium phosphate (PLB) expression in rats with myocardial ischemia reperfusion. Med Sci Monit. 2016;22:3309–15.
9. Yao L, Ping Y, Hua H, Fei W, Junquan Y, Lin S, et al. Anti-apoptotic effect of gastrodin through inhibiting serum deprivation-induced autophagy in rat H9C2 cardiomyocytes. Chin J N Drugs. 2016;25:328–34.
10. Yang P, Han Y, Gui L, Sun J, Chen YL, Song R, et al. Gastrodin attenuation of the inflammatory response in H9c2 cardiomyocytes involves inhibition of NF-kappaB and MAPKs activation via the phosphatidylinositol 3-kinase signaling. Biochem Pharmacol. 2013;85:1124–33.
11. Yang M, Linn BS, Zhang Y, Ren J. Mitophagy and mitochondrial integrity in cardiac ischemia-reperfusion injury. Biochim Biophys Acta Mol Basis Dis. 2019;1865:2293–302.
12. Maneechote C, Palee S, Kerdphoo S, Jaiwongkam T, Chattipakorn SC, Chattipakorn N. Balancing mitochondrial dynamics via increasing mitochondrial fusion attenuates infarct size and left ventricular dysfunction in rats with cardiac ischemia/reperfusion injury. Clin Sci. 2019;133:497–513.
13. Kuznetsov AV, Javadov S, Margreiter R, Grimm M, Hagenbuchner J, Ausserlechner MJ. The role of mitochondria in the mechanisms of cardiac ischemia-reperfusion injury. Antioxidant. 2019;8:E454.
14. Ong SB, Hausenloy DJ. Mitochondrial dynamics as a therapeutic target for treating cardiac diseases. Handb Exp Pharmacol. 2017;240:251–79.
15. Yang Y, Zhao L, Ma J. Penehyclidine hydrochloride preconditioning provides cardiac protection in a rat model of myocardial ischemia/reperfusion injury via the mechanism of mitochondrial dynamics mechanism. Eur J Pharmacol. 2017;813:130–9.
16. Tilokani L, Nagashima S, Paupe V, Prudent J. Mitochondrial dynamics: overview of molecular mechanisms. Essays Biochem. 2018;62:341–60.
17. Wang W, Fernandez-Sanz C, Sheu SS. Regulation of mitochondrial bioenergetics by the non-canonical roles of mitochondrial dynamics proteins in the heart. Biochim Biophys Mol Basis Dis. 2018;1864:1991–2001.
18. Paradies G, Paradies V, Ruggiero FM, Petrosillo G. Mitochondrial bioenergetics and cardiolipin alterations in myocardial ischemia-reperfusion injury: implications for pharmacological cardioprotection. Am J Physiol Heart Circ Physiol. 2018;315:H1341–52.
19. Suen DF, Norris KL, Youle RJ. Mitochondrial dynamics and apoptosis. Genes Dev. 2008;22:1577–90.
20. Li X, Huang Q, Wang M, Yan X, Song X, Ma R, et al. Compound K inhibits autophagy-mediated apoptosis through activation of the PI3K-Akt signaling pathway thus protecting against ischemia/reperfusion injury. Cell Physiol Biochem. 2018;47:2589–601.
21. Skehan P, Storeng R, Scudiero D, Monks A, McMahon J, Vistica D, et al. New colorimetric cytotoxicity assay for anticancer-drug screening. J Natl Cancer Inst. 1990;82:1107–12.
22. Cho SG, Xiao X, Wang S, Gao H, Rafikov R, Black S, et al. Bif-1 interacts with prohibitin-2 to regulate mitochondrial inner membrane during cell stress and apoptosis. J Am Soc Nephrol. 2019;30:1174–91.
23. Mishra P, Carelli V, Manfredi G, Chan DC. Proteolytic cleavage of Opa1 stimulates mitochondrial inner membrane fusion and couples fusion to oxidative phosphorylation. Cell Metab. 2014;19:630–41.
24. Chen Q, Chen X, Han C, Wang Y, Huang T, Du Y, et al. FGF-2 transcriptionally down-regulates the expression of BNIP3L via PI3K/Akt/FoxO3a signaling and inhibits necrosis and mitochondrial dysfunction induced by high concentrations of hydrogen peroxide in H9c2 cells. Cell Physiol Biochem. 2016;40:1678–91.
25. Li X, Zhu Q, Liu Y, Yang Z, Li B. Gastrodin protects myocardial cells against hypoxia/reoxygenation injury in neonatal rats by inhibiting cell autophagy through the activation of mTOR signals in PI3K-Akt pathway. J Pharm Pharmacol. 2018;70:259–67.
26. Li Y, Zhang Z. Gastrodin improves cognitive dysfunction and decreases oxidative stress in vascular dementia rats induced by chronic ischemia. Int J Clin Exp Pathol. 2015;8:14099–109.
27. Jiang G, Hu Y, Liu L, Cai J, Peng C, Li Q. Gastrodin protects against MPP^+-induced oxidative stress by up regulates heme oxygenase-1 expression through p38 MAPK/Nrf2 pathway in human dopaminergic cells. Neurochem Int. 2014;75:79–88.
28. Luo L, Kim SW, Lee HK, Kim ID, Lee H, Lee JK. Gastrodin exerts robust neuroprotection in the postischemic brain via its protective effect against Zn(2+)-toxicity and its anti-oxidative effects in astrocytes. Anim Cells Syst. 2018;22:429–37.
29. Liu S, Fang T, Yang L, Chen Z, Mu S, Fu Q. Gastrodin protects MC3T3-E1 osteoblasts from dexamethasone-induced cellular dysfunction and promotes bone formation via induction of the NRF2 signaling pathway. Int J Mol Med. 2018;41:2059–69.
30. Huang Q, Shi J, Gao B, Zhang HY, Fan J, Li XJ, et al. Gastrodin: an ancient Chinese herbal medicine as a source for anti-osteoporosis agents via reducing reactive oxygen species. Bone. 2015;73:132–44.
31. Cao YP, Zheng M. Mitochondrial dynamics and inter-mitochondrial communication in the heart. Arch Biochem Biophys. 2019;663:214–9.
32. Chen Y, Liu Y, Dorn GW 2nd. Mitochondrial fusion is essential for organelle function and cardiac homeostasis. Circ Res. 2011;109:1327–31.

33. Ong SB, Hall AR, Hausenloy DJ. Mitochondrial dynamics in cardiovascular health and disease. Antioxid Redox Signal. 2013;19:400–14.
34. Ong SB, Subrayan S, Lim SY, Yellon DM, Davidson SM, Hausenloy DJ. Inhibiting mitochondrial fission protects the heart against ischemia/reperfusion injury. Circulation. 2010;121:2012–22.
35. Chen L, Gong Q, Stice JP, Knowlton AA. Mitochondrial OPA1, apoptosis, and heart failure. Cardiovasc Res. 2009;84:91–9.
36. Karbowski M. Mitochondria on guard: role of mitochondrial fusion and fission in the regulation of apoptosis. Adv Exp Med Biol. 2010;687:131–42.
37. Frank S, Gaume B, Bergmann-Leitner ES, Leitner WW, Robert EG, Catez F, et al. The role of dynamin-related protein 1, a mediator of mitochondrial fission, in apoptosis. Devel Cell. 2001;1:515–25.
38. Abate M, Festa A, Falco M, Lombardi A, Luce A, Grimaldi A, et al. Mitochondria as playmakers of apoptosis, autophagy and senescence. Semin Cell Dev Biol. 2020;98:139–53.
39. Youle RJ, van der Bliek AM. Mitochondrial fission, fusion, and stress. Science. 2012;337:1062–5.
40. Li Y, Liu X. Novel insights into the role of mitochondrial fusion and fission in cardiomyocyte apoptosis induced by ischemia/reperfusion. J Cell Physiol. 2018;233:5589–97.
41. Liesa M, Shirihai OS. Mitochondrial dynamics in the regulation of nutrient utilization and energy expenditure. Cell Metab. 2013;17:491–506.
42. Schrepfer E, Scorrano L. Mitofusins, from mitochondria to metabolism. Mol Cell. 2016;61:683–94.
43. Liu X, Weaver D, Shirihai O, Hajnoczky G. Mitochondrial 'kiss-and-run': interplay between mitochondrial motility and fusion-fission dynamics. EMBO J. 2009;28:3074–89.
44. Anand R, Wai T, Baker MJ, Kladt N, Schauss AC, Rugarli E, et al. The i-AAA protease YME1L and OMA1 cleave OPA1 to balance mitochondrial fusion and fission. J Cell Biol. 2014;204:919–29.
45. Jofuku A, Ishihara N, Mihara K. Analysis of functional domains of rat mitochondrial Fis1, the mitochondrial fission-stimulating protein. Biochem Biophys Res Commun. 2005;333:650–9.
46. Zhang Y, Chan DC. Structural basis for recruitment of mitochondrial fission complexes by Fis1. Proc Natl Acad Sci USA. 2007;104:18526–30.
47. Loson OC, Song Z, Chen H, Chan DC. Fis1, Mff, MiD49, and MiD51 mediate Drp1 recruitment in mitochondrial fission. Mol Biol Cell. 2013;24:659–67.
48. Garcia I, Innis-Whitehouse W, Lopez A, Keniry M, Gilkerson R. Oxidative insults disrupt OPA1-mediated mitochondrial dynamics in cultured mammalian cells. Redox Rep. 2018;23:160–67.
49. Loboda A, Damulewicz M, Pyza E, Jozkowicz A, Dulak J. Role of Nrf2/HO-1 system in development, oxidative stress response and diseases: an evolutionarily conserved mechanism. Cell Mol Life Sci. 2016;73:3221–47.
50. Covas G, Marinho HS, Cyrne L, Antunes F. Activation of Nrf2 by H_2O_2: de novo synthesis versus nuclear translocation. Methods Enzymol. 2013;528:157–71.
51. Marinho HS, Real C, Cyrne L, Soares H, Antunes F. Hydrogen peroxide sensing, signaling and regulation of transcription factors. Redox Biol. 2014;2:535–62.
52. de Oliveira MR, Brasil FB, Furstenau CR. Evaluation of the mitochondria-related redox and bioenergetics effects of gastrodin in SH-SY5Y cells exposed to hydrogen peroxide. J Mol Neurosci. 2018;64:242–51.
53. Li Q, Niu C, Zhang X, Dong M. Gastrodin and isorhynchophylline synergistically inhibit MPP^+-induced oxidative stress in SH-SY5Y cells by targeting ERK1/2 and GSK-3beta pathways: involvement of Nrf2 nuclear translocation. ACS Chem Neurosci. 2018;9:482–93.
54. Zhao X, Zou Y, Xu H, Fan L, Guo H, Li X, et al. Gastrodin protect primary cultured rat hippocampal neurons against amyloid-beta peptide-induced neurotoxicity via ERK1/2-Nrf2 pathway. Brain Res. 2012;1482:13–21.
55. Liu XC, Wu CZ, Hu XF, Wang TL, Jin XP, Ke SF, et al. Gastrodin attenuates neuronal apoptosis and neurological deficits after experimental intracerebral hemorrhage. J Stroke Cerebrovasc Dis. 2020;29:104483.
56. de Oliveira MR, de Bittencourt Brasil F, Furstenau CR. Inhibition of the Nrf2/HO-1 axis suppresses the mitochondria-related protection promoted by gastrodin in human neuroblastoma cells exposed to paraquat. Mol Neurobiol. 2019;56:2174–84.
57. de Oliveira MR, Brasil FB, Furstenau CR. Nrf2 mediates the anti-apoptotic and anti-inflammatory effects induced by gastrodin in hydrogen peroxide-treated SH-SY5Y cells. J Mol Neurosci. 2019;69:115–22.
58. Liu S, Zhou L, Yang L, Mu S, Fang T, Fu Q. Gastrodin alleviates glucocorticoid induced osteoporosis in rats via activating the Nrf2 signaling pathways. Oncotarget. 2018;9:11528–40.
59. Qu LL, Yu B, Li Z, Jiang WX, Jiang JD, Kong WJ. Gastrodin ameliorates oxidative stress and proinflammatory response in nonalcoholic fatty liver disease through the AMPK/Nrf2 pathway. Phytother Res. 2016;30:402–11.
60. Zhang H, Yuan B, Huang H, Qu S, Yang S, Zeng Z. Gastrodin induced HO-1 and Nrf2 up-regulation to alleviate H2O2-induced oxidative stress in mouse liver sinusoidal endothelial cells through p38 MAPK phosphorylation. Braz J Med Biol Res. 2018;51:e7439.
61. Ong SB, Kalkhoran SB, Hernandez-Resendiz S, Samangouei P, Ong SG, Hausenloy DJ. Mitochondrial-shaping proteins in cardiac health and disease—the long and the short of it! Cardiovasc Drugs Ther. 2017;31:87–107.